Pergamon

Ultrasound in Med. & Biol., Vol. 20, No. 4, pp. 335–346, 1994

0301-5629/94 $6.00 + .00

0301-5629(94)E0007-Y

●*Original Contribution*

CLASSIFICATION OF LOWER LIMB ARTERIAL STENOSES FROM DOPPLER BLOOD FLOW SIGNAL ANALYSIS WITH TIME-FREQUENCY REPRESENTATION AND PATTERN RECOGNITION TECHNIQUES

ZHENYU GUO,[†‡] LOUIS-GILLES DURAND,[†] LOUIS ALLARD,[†]
GUY CLOUTIER[†] and HOWARD C. LEE[‡]

[†]Laboratory of Biomedical Engineering, Clinical Research Institute of Montreal, 110 Pine Avenue West, Montreal, Quebec, Canada, H2W 1R7; and [‡]Department of Electrical Engineering, McGill University, 3480 University Street, Montreal, Quebec, Canada, H3A 2A7

(*Received* 14 *June* 1993; *in final form* 5 *November* 1993)

Abstract—A pattern recognition system was used to classify Doppler blood flow signals for the determination of lower limb arterial stenoses. The diagnostic features were extracted from time-frequency representations of Doppler signals. Three techniques were tested to estimate time-frequency representations: the short-time Fourier transform, the autoregressive (AR) modeling, and the Bessel distribution. A boundary tracking algorithm was proposed to extract the frequency contour of the Doppler time-frequency representations. Based on the characteristics of the Doppler frequency contour, shape descriptors from an autoregressive analysis were proposed as diagnostic features. Simple algorithms were proposed to normalize these autoregressive shape descriptors. Amplitude distribution of the Doppler time-frequency representation was also found useful for stenosis classification. A total of 379 arterial segments from the aorta to the popliteal artery were classified by the pattern recognition system into three categories of diameter reduction (0–19%, 20–49%, and 50–99%). The short-time Fourier transform provided an overall accuracy of 80% (kappa = 0.38); AR modeling, 81% (kappa = 0.42); and the Bessel distribution, 82% (kappa = 0.43). All these results are better than those based on visual interpretation (accuracy = 76%, kappa = 0.29) performed by a trained technologist. The AR modeling and the Bessel distribution improved the performance of the pattern recognition system in comparison with the short-time Fourier transform. It is likely that with further improvement, the pattern recognition approach will be a useful clinical tool to quantify stenoses and to follow the disease progression with more reliability and less bias than visual interpretation as done currently in clinical practice.

Key Words: **Ultrasound, Doppler technique, Time-frequency representation, Lower limb arteries.**

INTRODUCTION

Ultrasonic duplex scanning has been proposed as a noninvasive alternative to angiography for the assessment of lower limb arterial stenoses (Jager et al. 1985; Kohler et al. 1987, 1990; Moneta et al. 1992; Ranke et al. 1992). Presently, the assessment of the degree of arterial diameter reduction is mainly performed by visual interpretation of the Doppler spectrogram based on the evaluation of the spectral waveform contour, the peak systolic frequency, the diastolic frequency, and the presence of spectral broadening during systole. The visual interpretation approach, although very useful in clinical practice, is difficult to use to objectively classify in quantitative terms the varying degrees of stenosis. Using computer analysis of Doppler blood flow signals, Allard et al. (1991) proposed a computer-based pattern recognition approach to classify the degrees of diameter reducing stenoses of the lower limb arteries. The diagnostic features were extracted from 379 Doppler spectrograms and classified into three categories of stenoses (0–19%, 20–49%, and 50–99% diameter reduction). Comparing with results based on angiography, their results showed that the pattern recognition approach was better than the visual interpretation approach.

Address correspondence to: Louis-Gilles Durand, Laboratory of Biomedical Engineering, Clinical Research Institute of Montreal, 110 Pine Avenue West, Montreal, Quebec, Canada, H2W 1R7.

Time-frequency representation of the Doppler blood flow signal

The Doppler blood flow signal has been shown to be a nonstationary random Gaussian signal (Bascom et al. 1993; Guo et al. 1993a). The spectrogram is a time-frequency representation (TFR) computed by using the short-time Fourier transform based on the assumption that the signal to be analyzed is stationary during a short time interval. The short-time Fourier transform has the advantages of having non-negative amplitude values and fast computation, but it has the main shortcoming of the tradeoff between time and frequency resolutions. Another TFR technique, based on autoregressive (AR) modeling, has been shown to be superior to the short-time Fourier transform due to its high frequency resolution (Guo et al. 1993b; Vaitkus et al. 1988). Recently new TFR techniques such as the Choi-Williams distribution (Choi and Williams 1989), the reduced interference distributions (Jeong and Williams 1992), and the Bessel distribution (Guo et al. 1994a) were developed to analyze nonstationary signals. These distributions describe how the frequency content of a signal is changing in time by mapping the signal into a joint time-frequency domain, instead of sectioning it into stationary intervals before computing the power spectra. A previous study based on simulated lower limb arterial Doppler blood flow signals showed that the Bessel distribution and AR modeling are better techniques for the computation of the Doppler TFR than the short-time Fourier transform (Guo et al. 1994b). In this study, we report the results to classify clinical Doppler blood flow signals based on these two new techniques compared with those obtained by using the spectrogram.

Feature extraction

An important problem related to Doppler blood flow signal analysis is to estimate the frequency contour of the Doppler TFR. Different computer-based algorithms have been proposed to extract this frequency contour (Allard et al. 1991; Cloutier et al. 1990; Mo et al. 1988). However, these algorithms work on the individual spectrum and need to find an optimal threshold to separate the Doppler signal from background noise. In the present study, image processing techniques were used to extract the frequency contour by representing it as a closed curve.

Another problem in using pattern recognition to classify lower limb arterial stenoses relates to the frequency-dependent features associated with blood flow velocities in the arteries. The blood flow velocity varies significantly from the aorta to the popliteal artery, and these variations require the design of a specific classifier for each arterial segment in order to optimize the performance of the pattern recognition system. By using this approach, the total population size must be subdivided into smaller subgroups, thus inevitably reducing the statistical reliability of the pattern recognition system. In Allard's work (1991), frequency scaling factors were applied to compensate for velocity variations by normalizing the frequency features as a function of maximal blood flow velocity of normal segments in order to design a single classifier for all the arterial segments investigated. However, due to variations in the individual patient's blood pressure, age, and vascular compliance, it may be difficult to obtain the frequency scaling factors with sufficient accuracy. It has been noticed that, although different arterial segments have different blood flow velocities, the morphological shapes of the frequency contours of the Doppler TFRs are very similar for a given degree of stenosis (Jager et al. 1985). In the present study, shape descriptors were used as features for the pattern recognition system. Since shape descriptors are independent of the shape size, normalization with respect to blood flow velocities of different arterial segments and different patients is not required.

In summary, this paper describes a pattern recognition system based on the shape descriptors and amplitude distribution features extracted from the TFRs of Doppler blood flow signals for objective classification of lower limb arterial stenoses. The classifier was designed to categorize arterial stenoses into three classes: 0–19%, 20–49%, and 50–99% diameter reduction. All arterial segments studied from aorta to popliteal artery were classified using a single classifier. The results were compared blindly with those of angiography.

MATERIALS AND METHODS

Patient population and data acquisition

The database used in this study is the same as that used by Allard et al. (1991). Subjects were recruited among patients referred to the Montreal Hotel-Dieu Hospital for the conventional biplane contrast arteriographic examination of the lower limb arteries. For arteriographic studies, each angiographic film was read by an experienced angioradiologist and the view showing the most severe lesion was used to estimate the percentage of the diameter-reducing lesion. On the basis of caliper measurements of the normal and residual arterial diameter of each segment, the severity of the disease was classified into 5 classes (normal, 1–19%, 20–49%, 50–99% diameter reduction, and occlusion). The 37

Table 1. Doppler spectrogram classification.

Angiographic category	Doppler criteria
Normal	Tri- or biphasic waveform Systolic window present No spectral broadening
1–19% diameter reduction	Peak systolic velocity and waveform within normal range Spectral broadening present
20–49% diameter reduction	30–50% increase in peak systolic velocity Reverse flow component present
50–99% diameter reduction	50–100% increase in peak systolic velocity Reverse flow component absent Extensive spectral broadening
Occluded	No flow detected in vessel

Note: Permission to reprint this table, from Taylor et al. 1988, p. 332, was obtained from Raven Press.

patients included in the Doppler study are those whose arteriographic examination was performed within 3 months (32 less than 2 months and 5 between 2 and 3 months). Doppler studies were performed with an ATL Ultramark 8 duplex scanner which combines real-time B-mode imaging and pulsed Doppler blood flow recording system. The B-mode image was used to identify the vessel of interest, to place the pulsed Doppler sample volume in the center-stream of the vessel, and to maintain a standard angle of incidence of 60 degrees between the Doppler beam and blood vessel axis. The arterial segments examined in each limb were: the distal aorta, the common and external iliac arteries, the common and profunda femoral arteries, the superficial femoral artery, and the popliteal artery above the knee. A mechanically oscillating probe, operating at 5 MHz, was used for all Doppler recordings. According to the manufacturer's specifications, the sample volume used for all recordings had a length of 1.5 mm in the direction of the axial beam, which is much smaller than the diameter of the arterial segments studied. Doppler signals from all segments were recorded at midcourse of the segment if normal or at the site of most severe disease. The latter was identified by the technologist as the site having maximal flow velocity. In order to standardize the recordings, the patients were asked to rest supine at least 30 min in a controlled temperature environment (21–23°C). The criteria proposed by Jager et al. (1985) and presented in Table 1 (Taylor et al. 1988) were used to grade arterial stenoses into the above 5 classes by visual interpretation of a technologist. The Doppler spectrograms of normal and three different degrees of stenoses are shown in Fig. 1.

The two quadrature Doppler blood flow signals were recorded for a period of approximately 20 s on a four-channel audio type recorder (TASCAM 22-4) for off-line analysis. The ECG signal was also recorded on a FM channel and used to detect the beginning of each cardiac cycle. Voice comments indicating the patient's name and the sites analyzed were recorded on the fourth channel of the recorder. The high-pass filter used to remove the wall motion was set at 100 Hz. During tape playback, ECG and Doppler signals were digitized with a 12-bit A/D converter (DT-2828 board) at sampling rates of 2 kHz and 20 kHz, respectively. Before digitization, Doppler blood flow signals were low-pass filtered at 9 kHz with eighth-order Butterworth filters (−48 dB/octave) to prevent frequency aliasing. The cut-off frequency of 9 kHz was always greater than half of the Pulse Repetition Frequency (PRF) used by the Doppler system. During Doppler signal acquisition, an algorithm for QRS-complex detection was used to locate the beginning of each cardiac cycle and synchronize the analysis of the Doppler signals. The mean heart rate was also computed and used to reject all beats with an interval differing by more than 10% from the mean heart rate duration.

Time-frequency representation (TFR) of Doppler blood flow signals

In the present study, Doppler TFRs based on the short-time Fourier transform, AR modeling, and the Bessel distribution (BD) were computed. Doppler signals were analyzed in a period of 700 ms after the QRS-complex of the ECG for each cardiac cycle. To compute Doppler TFRs, a time increment of 5 ms was used and each spectrum had 256 samples. Consequently, the Doppler TFR was a matrix with the dimension of 140 × 256. For each arterial segment, an average TFR was obtained by averaging 5 individual TFRs from a series of cardiac cycles in synchronization with the QRS-complex. As pointed out by Guo et al. (1994b), time-frequency representations are sensitive to the values of parameters (such as window length) used for computation. In the present study, those values of parameters optimized in the work of Guo et al. (1994b) for Doppler signal analysis were used.

The spectrogram. The basic approach to compute the spectrogram is to find the power density of the signal at time n by analyzing a small segment of the signal around n. Specifically, the signal is multiplied by a window function $w(n)$ centered at time n, and the Fourier transform of the windowed signal is calculated by

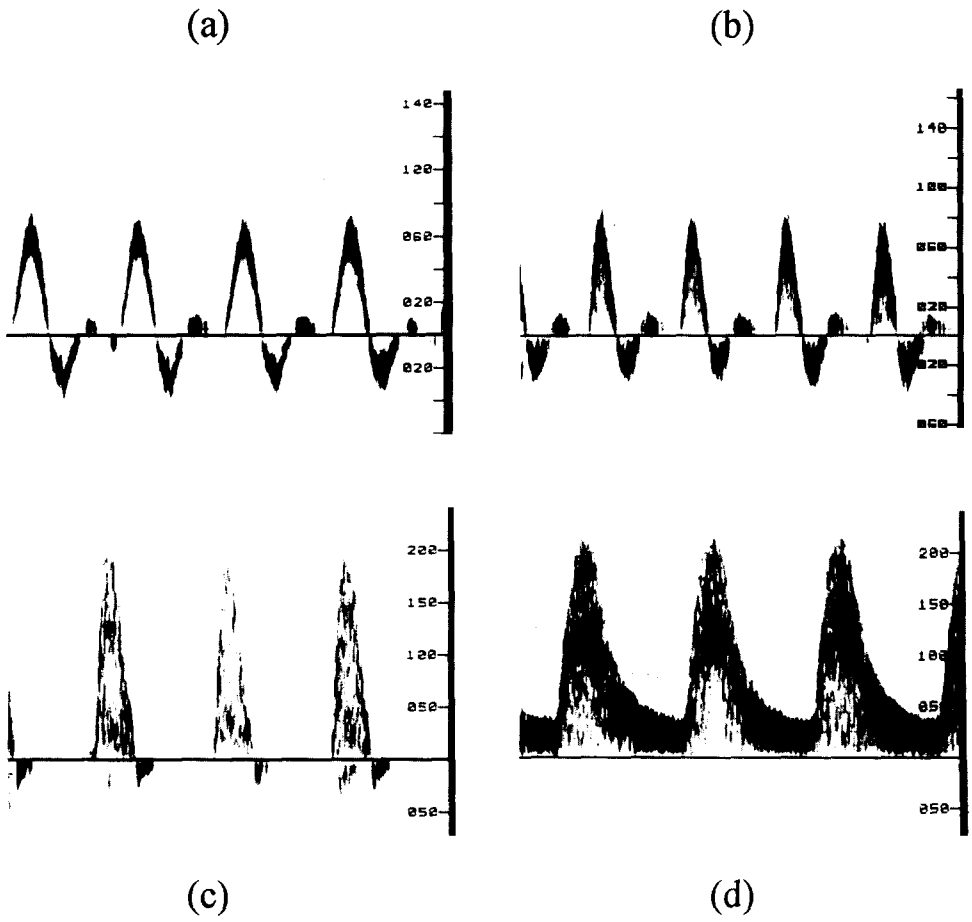

Fig. 1. Examples of Doppler Fourier spectrograms for different arteriographic categories of arterial stenoses: (a) normal, (b) <20% diameter reduction, (c) 20–49% diameter reduction, (d) 50–99% diameter reduction.

$$X_n(k) = \sum_{m=0}^{N-1} x\left(m + n - \frac{N}{2}\right) w\left(m - \frac{N}{2}\right) e^{-j\frac{2\pi k}{N}m} \quad (1)$$

where k is the frequency and N is the window length. The spectrogram of the Doppler signal $x(n)$ is then computed by

$$\mathrm{SPEC}_x(n, k) = |X_n(k)|^2. \quad (2)$$

An 8 ms Hanning window was used in the computation of the Doppler spectrogram.

The autoregressive modeling. It has been shown that the quadrature Doppler signal can be modeled by a complex time-varying AR process (Guo et al. 1993b). Here we recall the equation used to compute the TFR of the time-varying AR modeling as

$$\mathrm{AR}_x(n, k) = \frac{\delta_p^2(n)}{\left|1 + \sum_{m=1}^{p} a(m, n)\exp\left(-j\frac{2\pi k}{N}m\right)\right|^2} \quad (3)$$

where p is the model order, $a(m, n)$ are complex time-varying coefficients, and $\delta_p^2(n)$ is the variance of the modeling error. The complex coefficients $a(m, n)$ were computed by using the Yule–Walker equations together with the Levinson–Durbin algorithm (Kay and Marple 1981). In the present study, a 14 ms rectangular window was used to generate Doppler TFRs, and the "Akaike's information criterion" (AIC) (Kay and Marple 1981) was used to determine the model order p for every spectrum.

The Bessel distribution. The Bessel distribution (BD) is a member of Cohen's class of time-frequency

distribution with a Bessel function kernel. The alias-free BD can be expressed as (Guo et al. 1994a)

$$\mathrm{BD}_x(n, k) = 2 \sum_{\tau=-\infty}^{+\infty} w_N(\tau) e^{\frac{-j2\pi k\tau}{N}} \left[\sum_{\mu=(-\tau-2\alpha|\tau|)/2}^{(-\tau+2\alpha|\tau|)/2} \frac{2}{\pi\alpha|\tau|} \sqrt{1 - \left(\frac{2\mu + \tau}{2\alpha\tau}\right)^2} \; x(n + \mu + \tau)x^*(n + \mu) \right] \quad (4)$$

where α is a parameter to determine a tradeoff between auto-term resolution and cross-term reduction. In the present study, window $w_N(\tau)$ was a 4 ms sine-cosine window and α had a value of 14.5. Examples of average Doppler TFRs computed by using the short-time Fourier transform, AR modeling, and the BD are presented in Fig. 2.

Frequency contour extraction

As mentioned previously, a critical problem with Doppler blood flow signal analysis is to extract the frequency contour of the Doppler TFR. The algorithms proposed in the literature are based on estimating the maximum and minimum frequencies of each individual spectrum (Allard et al. 1991; Cloutier et al. 1990; Mo et al. 1988). One limitation with this approach is how to determine properly the background noise level since the algorithms try to separate spectral segments containing blood flow signal from those containing noise. By using image processing techniques, Allard et al. (1992) showed better results to extract the frequency contour. In the present study, the Doppler TFRs were converted into 256 gray-level images and the Laplacian edge detector was used to extract the edges of images. As the Laplacian edge detector tends to produce false edges due to noise, the images were first smoothed by preprocessing. A mean filter of size 3 × 3 was first applied for smoothing the Doppler speckle and background noise. A median filter of size 3 × 3 was then applied for further improvement. The median filter has the property of preserving edges and suppressing residual noise of local fluctuations. Using a threshold of 5% of maximal gray level, a binary image was generated from the smoothed image. The edge image was obtained by performing Laplacian edge detection on the binary image.

The Laplacian edge detector normally produces "thick" edges. In the present study, the outer boundary of the edge was used to represent the frequency contour. Using *a priori* knowledge that the Doppler frequency contour is a closed curve, only one closed contour for each TFR was obtained, and in this way the residual background noise peaks were eliminated. The contour extraction algorithm is described as follows. In Fig. 3, a 3 × 3 window shows the current contour point P_c and its 8 neighbors P_0–P_7. The contour tracking was started by identifying the first contour point as the first no-zero point found on the Laplacian edge image by searching from zero frequency at the QRS timing reference of the ECG, and initializing a

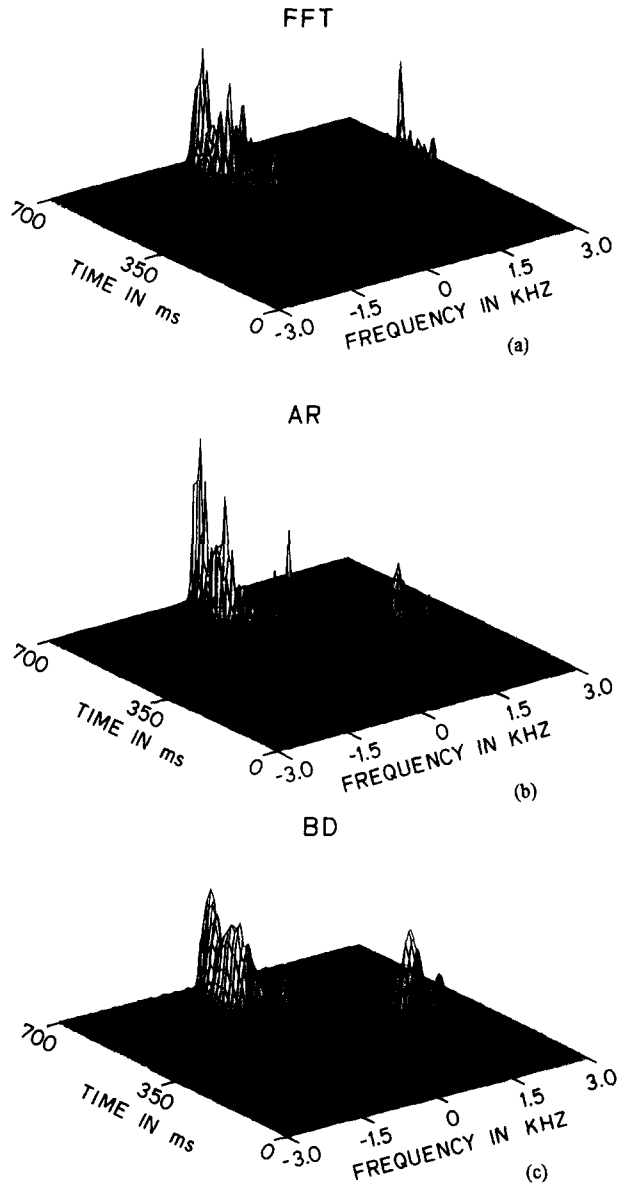

Fig. 2. Doppler TFRs of an arterial segment having a 0–19% diameter reduction: (a) short-time Fourier transform, (b) time-varying AR modeling, and (c) Bessel distribution.

direction code which keeps the interior of the contour to the left of the tracking direction. The directional codes from 0–7 were used to specify the direction in which a step must be taken to go from the current contour point to the next. Then, we began the iterative process of finding the next contour point, given the current point P_c and the tracking direction. Working in the 3 × 3 window centered on the current contour point, the next contour point was taken from three candidate points, the neighbor specified by the directional code and the neighbors on each side of it. For example, the candidates of the next contour point are P_7, P_0, and P_1 if current directional code is 0, and P_0, P_1, and P_2 if current directional code is 1. The next contour point was the first no-zero point of these three candidates evaluated in a counterclockwise direction. When the next contour point was found, recoding the directional code as the direction from current to next contour points was performed. This iterative process was continued until a closed contour was generated.

Diagnostic feature extraction and selection

A total of 15 raw diagnostic features were extracted from the average Doppler TFRs of each arterial segment. The frequency contour was used as a mask on the original Doppler TFRs and all features were extracted on and within this contour. The 15 features are described next.

Ratio of spectral envelope areas. Cannon et al. (1982) demonstrated the diagnostic value of the spectral envelope area (SEA) for determining the stenosis of the aortic valve. SEA is defined as the area between the minimum and maximum frequency curves and directly reflects the spectral broadening of the Doppler TFR. Because of large interindividual variability of blood flow velocities from the aorta to the popliteal artery, a standard threshold value of SEA cannot be defined with sufficient accuracy for a specific degree

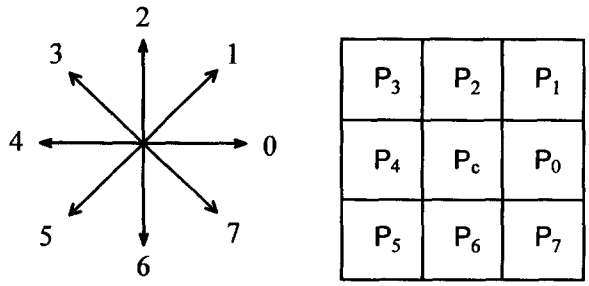

Fig. 3. A 3 × 3 window illustrating the current pixel P_c and the 8 directional codes used to extract the frequency contour of Doppler TFR (see text for details).

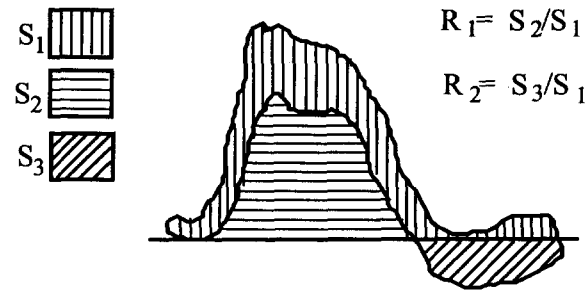

Fig. 4. Illustrating the definition of area ratios R1 and R2 by using the frequency contour of the TFR in Fig. 2c.

of stenosis. In the present study, an area ratio R1, as defined in Fig. 4, was used as a feature to estimate the spectral broadening. Furthermore, according to Jager et al. (1985), the loss of reverse blood flow could indicate the presence of hemodynamically significant stenosis, and thus an area ratio R2 (shown in Fig. 4) was used to reflect this phenomenon. Since they are area ratios, R1 and R2 are independent to the variability of blood velocity of different arterial segments and patients.

AR shape descriptors. As mentioned previously, the assessment of lower limb arterial stenoses by using ultrasonic duplex scanning is mainly performed by visual interpretation of the Doppler time-varying spectra (Doppler TFR). Visual interpretation is mostly based on the shape of the TFR. This observation motivates the use of shape descriptors as diagnostic features. The shape descriptors of a closed contour should be invariant to changes of its size, position, and orientation. That is, two closed contours have the same shape descriptors if one can be obtained from another by scaling, translation, and rotation in the image plane (Kashyap and Chellappa 1981). Different degrees of stenosis have different frequency contours as shown in Fig. 1. Those criteria described in Table 1 are applicable to all the segments from the aorta to the popliteal artery (Jager et al. 1985), except that they have different peak systolic frequency (peak systolic blood flow velocity). For different arterial segments, the frequency contours should have similar shape descriptors if they belong to the same class of stenosis. Therefore, the shape descriptors of the Doppler TFR frequency contour can be used as features for the classification of varying degrees of stenoses, and no compensation for velocity variation with respect to segment and patient is required. In the following paragraph, the procedure to compute the shape descriptors will be presented. The frequency contour will be first represented by a one-dimensional sequence, and then algorithms to nor-

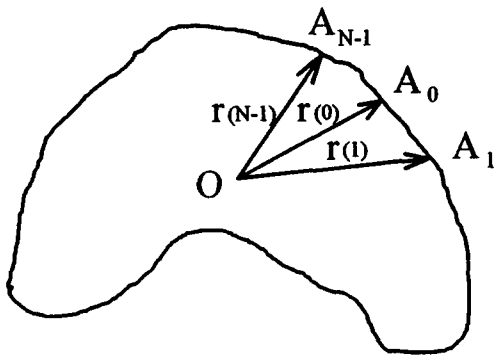

Fig. 5. Time sequence representation of a closed contour.

malize this sequence with respect to size and position of the corresponding frequency contour and to the starting point of the sequence will be proposed.

There are several basic methods of closed contour representation in the literature such as Cartesian coordinates (Persoon and Fu 1977) or relative angular bend (Oliviero and Scarpetta 1981) as functions of arc length. In the present study, the method proposed by Kashyap and Chellappa (1981) was used to represent the frequency contour by a 1-D sequence $\{r(n)\}$ of radial distances measured from the centroid to each point of the contour. As shown in Fig. 5, let the contour points be A_0–A_{N-1}, the centroid of the contour be O, and $OA_n = r(n)$, the required sequence is $\{r(0), r(1), \ldots, r(N-1)\}$. Since the contour is closed,

$$r(N+n) = r(n) \quad \forall \text{ integer } n, \tag{5}$$

and $r(n)$ is a periodic sequence with the period N. In the present study, all contours were represented by 512 equidistant points generated through the Fourier transform of the original sequence, and then taking the inverse Fourier transform with appropriate zero-padding in the frequency domain. This number of samples were considered sufficient to provide the needed resolution in our application. Figure 6 shows the frequency contour and the corresponding sequence $\{r(n)\}$ of the Doppler TFR shown in Fig. 2c.

Since the duration between the QRS-complex and the peak systole varies among patients, the frequency contour is position-dependent in the image plane. However, the sequence $\{r(n)\}$ is already invariant with respect to the position of the corresponding contour since the centroid of the contour is used as reference. Thus, we only need to normalize $\{r(n)\}$ with respect to the shape, size and orientation. The normalization of the size can be obtained by dividing each element of the sequence by the mean value of that sequence. Specifically,

$$x(n) = r(n)/\bar{r}, \quad 0 \le n \le 511 \tag{6}$$

where

$$\bar{r} = \frac{1}{512} \sum_{n=0}^{511} r(n). \tag{7}$$

The resulting sequence $\{x(n)\}$ is a size invariant version of sequence $\{r(n)\}$.

Now regarding orientation, our frequency contours actually do not have any orientation problem in the image domain. However, the 1-D sequence could be generated from any starting point on the contour. The normalization of $\{x(n)\}$ with respect to its starting point should be addressed. In fact, normalizing the sequence $\{x(n)\}$ with respect to shape orientation is equivalent to normalizing it with respect to its starting point. There are many algorithms for this purpose (*e.g.*,

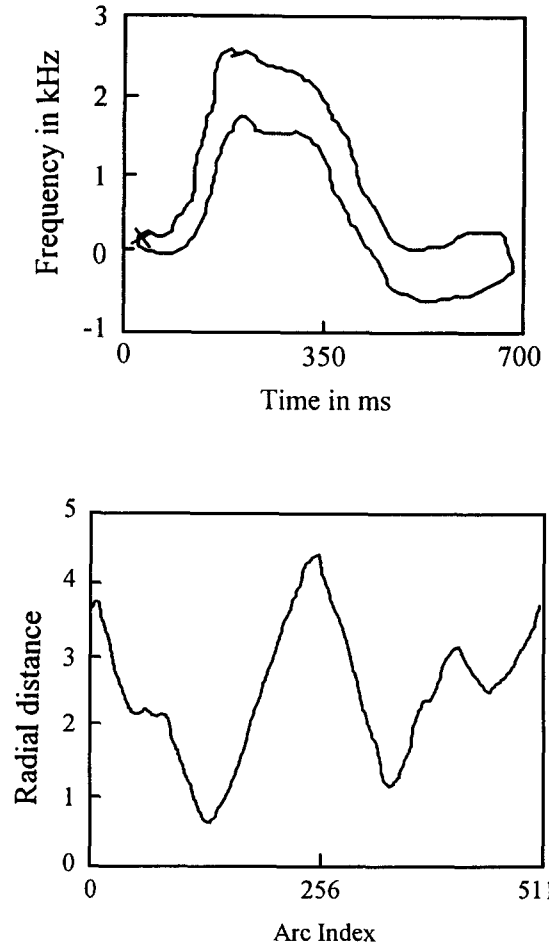

Fig. 6. The Doppler frequency contour and the time sequence of the Doppler TFR shown in Fig. 2c. The starting point is marked by X on the frequency contour.

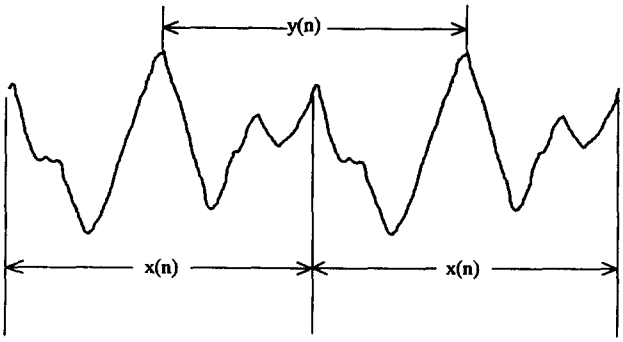

Fig. 7. Normalization of the time sequence with respect to the starting point.

Persoon and Fu 1977; Wallace and Wintz 1980). In the present study, a straightforward method was proposed. Because the sequence $\{x(n)\}$ is known to be periodic, another period of $\{x(n)\}$ was appended and a new sequence $\{y(n)\}$ was taken as the section between two maximum radial distance points in two connective periods of $\{x(n)\}$, as shown in Fig. 7. The sequence $\{y(n)\}$ is thus invariant to shape, size, and position, as well as to its starting point.

To obtain the shape descriptors, the sequence $\{y(n)\}$ was modeled as an AR process,

$$y(n) = \sum_{i=1}^{p} a_i y(n-i) + e(n) \qquad (8)$$

where p is the model order, a_i are the AR coefficients, and $e(n)$ is the modeling error which is a zero mean white Gaussian process. In the present study, the AR model order was arbitrarily selected as 7. The variance σ^2 of the error and the AR coefficients $a1$–$a7$ were called AR shape descriptors used as diagnostic features for classifying the stenoses.

Amplitude distribution features. According to the work of Cloutier et al. (1991), the amplitude distribution of the Doppler TFR contains important information to classify the stenosis. Five features related to the amplitude distribution or gray level distribution of the Doppler TFR were used in the present study.

The normalized second-order central moments η_{11}, η_{02}, and η_{20} (Gonzalez and Wintz 1977) of the Doppler TFR were first used as features to describe its amplitude distribution. These features reflect how gray levels of the Doppler TFR are distributed around its center of gravity. Let the Doppler TFR be described by TFR(n, k). Then,

$$\eta_{pq} = \mu_{pq}/\mu_{00}^{\gamma} \qquad (9)$$

where

$$\gamma = \frac{p+q}{2} + 1, \quad p+q = 2, 3, \cdots$$

$$\mu_{pq} = \sum_n \sum_k (n-\bar{n})^p (k-\bar{k})^q \mathrm{TFR}(n,k) \qquad (10)$$

and $(\bar{n}, \bar{k})$ is the center of gravity of the Doppler TFR.

Another way to describe the image amplitude distribution is the one-dimensional gray level histogram. The mean and variance of the Doppler TFR gray level histogram were used as another two features:

$$\mathrm{gmean} = \sum_{i=0}^{255} ip(i) \qquad (11)$$

$$g\mathrm{var} = \sum_{i=0}^{255} (i - \mathrm{gmean})^2 p(i) \qquad (12)$$

where $p(i)$ is the gray level histogram of the image.

All 15 features were considered to have discriminant power. In the present study, the best discriminant feature pattern was considered to be the pattern producing the best classification accuracy. It was selected by evaluating all diagnostic patterns composed of a number of features varying between 2 and a value equal to a ratio $N_i/5$, where N_i is the minimum number of samples among classes. This ratio was recommended in the past to minimize the risk of overestimating the real performance of the classifier (Jain 1987).

Classifier design and evaluation

A Bayes classifier developed by Durand et al. (1988) was used in this study. From the statistical point of view, this classifier represents the optimum measure of performance with known feature distribution. The conventional biplane contrast angiographic studies were used as the "gold standard" to evaluate the performance of the classifier.

The Bayes classifier is represented in the term of a set of discriminant functions $g_i(X)$, $i = 1, \ldots, k$, where k is the number of classes. The classifier assigns a feature vector X to class ω_i if $g_i(X) > g_j(X)$ for all $j \neq i$. By assuming that the feature vectors X within the ith class $P(X/\omega_i)$ have a multivariate Gaussian distribution with mean vector μ_i and covariance matrix C_i, the discriminant functions for the Bayes classifier are

$$g_i(X) = -\tfrac{1}{2}(X-\mu_i)^t C_i^{-1}(X-\mu_i) - \tfrac{1}{2}\log|C_i| + \log P(\omega_i) \qquad (13)$$

where $P(\omega_i)$ is the *a priori* probability of class ω_i.

In the present study, unknown data were classified

Table 2. Duplex scanning (visual interpretation) compared with angiography for lower limb arterial disease classification.

	Duplex classification			
Angiography	0–19%	20–49%	50–99%	Total
0–19%	**265**	21	2	288
20–49%	43	**7**	5	55
50–99%	13	5	**18**	36
Total	321	33	25	379
Accuracy = 76%		Kappa = 0.29		

Note: Permission to reprint this table was obtained from Ultrasound Med. Biol.

by a pattern recognition system based on the Bayes classifier into three classes (0–19%, 20–49%, and 50–99% diameter reduction) according to the following binary decision rule:

DECIDE greater versus less than 50% stenosis

IF less than 50% stenosis, THEN DECIDE

greater versus less than 20% stenosis.

The leave-one-out method (Toussaint 1974) was used to evaluate the performance of the classifier. By using this method, the training set consisting of the complete patient population minus one is used to design the classifier, and the remaining patient is then classified. The procedure is repeated by extracting one patient at a time until all patients have been classified individually. The kappa statistic (Cohen 1960) was computed to measure the agreement between the pattern recognition system and angiography. If the agreement is greater or equal to chance, the kappa value will be greater or equal to zero, with a maximum value of +1 for a perfect agreement. Similarly, if the agreement is less than chance agreement, the kappa value will be negative.

RESULTS

Complete examinations by ultrasonic duplex scanning and arteriography were performed on 37 patients with ages between 21 to 79 years (58 ± 15). There were 379 segments available for computer analysis (Allard et al. 1991). Based on the evaluations of arteriography, 288 (76%) had a 0–19% diameter reduction stenosis, 55 (15%) had a 20–49% stenosis, and 36 (9%) had a 50–99% stenosis. Among the latter, 23 were associated with the presence of severe disease (50–100% stenosis) in other adjacent (proximal and/or distal) segments.

The results by visual interpretation of the Doppler spectral waveforms are first shown in Table 2 as a two-way contingency table in order to compare with the pattern recognition results. An accuracy of 76% was obtained with a kappa value of 0.29 between the Doppler technologist and the angioradiologist. Of the 288 segments in the 0–19% class, 92% (265/288) were correctly classified. Of the 55 segments in the 20–49% class, 13% (7/55) were correctly classified. Of 36 segments in the 50–99% class, 50% (18/36) were correctly classified.

The best results obtained by the pattern recognition system with three different TFR techniques are presented in Tables 3, 4, and 5, respectively. The most discriminant features used at each binary decision branch by the pattern recognition system are also listed. Since the minimum number of segments was 36 in the 50–99% class, no feature pattern size greater than 7 was tested in order to satisfy a sample size to feature size ratio greater than 5. As shown in Table 3, when the short-time Fourier transform was used to compute the Doppler TFR, the overall accuracy was 80% and the kappa value was 0.38. Of the 288 segments in the 0–19% class, 96% (276/288) were correctly classified. Of the 55 segments in the 20–49% class, 16% (9/55) were correctly classified. Of 36 segments in the 50–99% class, 53% (19/36) were correctly classified. When AR modeling was used to compute the Doppler TFR, the results from Table 4 show an overall accuracy of 81% and a kappa value of 0.42. Among the segments tested, 94% (272/288) were correctly classified as the 0–19% class, 16% (9/55) were correctly classified as the 20–49% class, and 67% (24/36) were correctly classified as the 50–99% class. As shown in Table 5, when Bessel distribution was used to compute the Doppler TFR, an overall accuracy of 82% and kappa value of 0.43 were obtained. Overall, 97% (280/288) of segments were correctly classified as the 0–19% class, 15% (8/55) of segments were correctly classi-

Table 3. Pattern recognition of Doppler signals compared with angiography for lower limb arterial disease classification. FFT was used to compute Doppler TFRs.

	Pattern recognition (FFT)			
Angiography	0–19%	20–49%	50–99%	Total
0–19%	**276**	8	4	288
20–49%	42	**9**	4	55
50–99%	14	3	**19**	36
Total	332	20	27	379
Accuracy = 80%		Kappa = 0.38		

Most discriminant features at the first binary decision branch: σ^2, $a2$, $a3$, $g$var, η_{02}, η_{20}. Most discriminant features at the second binary decision branch: σ^2, $a3$, $g$mean, η_{11}.

Table 4. Pattern recognition of Doppler signals compared with angiography for lower limb arterial disease classification. AR modeling was used to compute Doppler TFRs.

	Pattern recognition (AR)			
Angiography	0–19%	20–49%	50–99%	Total
0–19%	**272**	8	8	288
20–49%	43	**9**	3	55
50–99%	11	1	**24**	36
Total	326	18	35	379
Accuracy = 81%		Kappa = 0.42		

Most discriminant features at the first binary decision branch: R1, $a2$, gmean, gvar. Most discriminant features at the second binary decision branch: R1, σ^2, $a1$, $a2$, η_{20}.

fied as the 20–49% class, and 61% (22/36) of segments were correctly classified as the 50–99% class.

Comparing the results presented in Tables 2, 3, 4, and 5, it is obvious that the pattern recognition system is better than the visual interpretation approach to classify the lower limb arterial stenoses. The new TFR techniques (the AR modeling and the Bessel distribution) improved the classification results. The results in Table 3 are similar with those of Allard et al. (1991) (accuracy of 81%, kappa value of 0.35). This indicates that the diagnostic features proposed in the present study are as good as those normalized with respect to blood flow velocity.

DISCUSSION

Angiography has been, for a long time, the definitive test for lower limb arterial stenoses determination. However, this approach provides anatomic rather than hemodynamic information and has important limitations. Interpretation is subjected to interobserver variability (Jager et al. 1985). Furthermore, due to the invasive nature and relatively high cost, it is not suitable for screening purposes and disease follow-up. As an alternative, ultrasonic duplex scanning is a good noninvasive tool. Jager et al. (1985) showed that the agreement between duplex scanning and angiography was as good as the agreement between two radiologists reading the same angiograms. Although color-flow duplex scanning has several advantages over the conventional duplex technique to localize turbulent flow, it still remains necessary to perform Doppler spectral analysis to grade arterial stenosis. In clinical practice, the Doppler spectra are very complex and not as clear as those typical patterns shown in Fig. 1. Visual interpretation of spectral patterns as currently done with the duplex scanner is not sufficient. Thus, the use of a pattern recognition system to classify Doppler blood flow signals for the determination of lower limb arterial stenoses is logical. It is possible to quantify complex Doppler spectral patterns and eliminate visual interpretation bias so as to increase the diagnostic accuracy.

It is well recognized that selecting optimal Doppler blood flow signals is a crucial step prior to signal processing and waveform classification. The technologist performing the duplex scanning is of primary importance and needs to be well trained to perform the scanning competently. A firm understanding of equipment controls, anatomy, and physiology of blood flow is essential for an accurate scanning technique. Interobserver and intraobserver variability in the measurement of Doppler signal has also been noticed. It is thus of importance to standardize the examination technique for all patients to obtain reliable Doppler signals for stenosis classification.

The technique used to compute the Doppler TFR also plays an important role in Doppler blood flow signal analysis. For historical reasons, the short-time Fourier transform has been the major technique for this purpose. It has for a long time been argued that this technique cannot provide sufficient information to reflect the nonstationary variations of the blood flow in the cardiovascular system. Furthermore, due to the random nature of the Doppler blood flow signal and the statistical variation of the technique itself, it was expected that the short-time Fourier transform could smear mild disease in the Doppler TFR. It has been shown (Vaitkus et al. 1988) that other techniques for spectral analysis, such as AR and ARMA modeling, offer the potential for achieving significant improvement in the display of the Doppler spectral waveform when compared to the short-time Fourier transform approach. In a previous study, using computer-simulated lower limb arterial Doppler blood flow signals,

Table 5. Pattern recognition of Doppler signals compared against angiography for lower limb arterial disease classification. The Bessel distribution was used to compute Doppler TFRs.

	Pattern recognition (BD)			
Angiography	0–19%	20–49%	50–99%	Total
0–19%	**280**	1	7	288
20–49%	42	**8**	5	55
50–99%	14	0	**22**	36
Total	336	9	34	379
Accuracy = 82%		Kappa = 0.43		

Most discriminant features at the first binary decision branch: R1, σ^2, $a2$, gvar, η_{02}. Most discriminant features at the second binary decision branch: R1, R2, $a3$.

we compared five methods to compute the Doppler TFR and found that the Bessel distribution and the AR modeling are better than the short-time Fourier transform (Guo et al. 1994b). The clinical application in the present study confirmed this conclusion. For instance, we have shown by kappa statistics that both the Bessel distribution and the AR modeling improve the assessment of arterial stenoses, although the improvements are not very significantly due to the possible reasons discussed later. The results obtained by Bessel distribution are similar with those obtained by AR modeling.

It should be noticed that the classification of a particular segment into a class of stenosis is based on an imperfect "gold standard": angiography. In classifying lower limb arteries into five classes, Jager et al. (1985) reported that the agreement between two angioradiologists reading independently the same films was only 70%. Therefore, the limitation of angiography presents a significant problem in the evaluation of the proposed approach. Another reason that could explain the limited performance of our approach is the presence of multiple stenoses in some of the patients. As previously mentioned, among 36 segments within 50–99% stenosis, there were 23 associated with the presence of severe disease (50–100%) in proximal and/or distal segments. We have noticed that the presence of disease adjacent to the segment of interest could change the pattern of Doppler TFR of that segment, which resulted in misclassification of stenosis. An additional analysis has been done by Allard et al. (1994) to investigate the limitations of duplex scanning for diagnosing lower limb arterial stenoses in the presence of adjacent segment disease. It was found that the presence of multiple stenoses decreases significantly the accuracy of the duplex scanning for the detection and quantification of lower limb arterial stenoses. To gain more understanding of the amplitude distribution of Doppler TFR and the effect of multiple stenoses, a flow loop model has been recently set up in our laboratory to perform basic experimental measurements.

The algorithm proposed to extract the frequency contour was proven robust. It overcame the possible erratic frequency contour sometimes observed when extracted from individual spectrum and facilitated the representation of the shape sequence. The motivation to use shape descriptors as diagnostic features is based on the importance of shape to the human visual system during interpretation of the Doppler spectral waveform. In the present application, we believe that AR shape descriptors are better than other shape descriptors, such as Fourier descriptors (Persoon and Fu 1977). This is because a fixed number of AR descriptors can represent all contours in a shape class (a class of stenosis). The differences between shapes in the same class manifest themselves as different sample sequences of the modeling error. The frequency contours of same degree of stenosis have small variations among arterial segments, but their AR descriptors are relatively stable.

We also tried to classify stenoses by using only AR shape descriptors as well as two area ratios (R1 and R2) of Doppler TFRs computed by using the Bessel distribution. An accuracy of 79% and a kappa value of 0.37 were obtained which were better than those reported in Table 2 by using visual interpretation but not as good as those reported in Table 5 by using all features. This demonstrated that the amplitude distribution of Doppler TFR also contains important diagnostic features. Work done by Cloutier et al. (1991) suggested the importance of amplitude distribution of Doppler spectra for the classification of stenoses. However, these amplitude-related features cannot be extracted from visual interpretation. This again suggests to use computer analysis and pattern recognition system to improve stenosis classification.

CONCLUSION

Two new techniques for Doppler TFR estimation, the AR modeling and the Bessel distribution, were tested using clinical Doppler blood flow signals for lower limb arterial stenoses classification. Results showed that these two techniques are better than the conventional short-time Fourier transform. An algorithm based on image processing techniques was proposed to extract the frequency contour from Doppler TFRs. This algorithm was shown to be robust. AR shape descriptors were proposed as diagnostic features. Simple algorithms to normalize the shape descriptors were implemented and confirmed valuable in this clinical application. Advanced investigations in understanding amplitude features and multiple stenoses will be carried out in the near future. It is likely that with continued improvement, the pattern recognition approach will be feasible to detect stenoses and to follow the disease progression with more reliability and less bias than visual interpretation.

Acknowledgements—Authors gratefully acknowledge the technical assistance of Gaetan Boudreau and Rejean Senecal as well as the secretarial assistance of Francine Durand. This research was supported by Natural Sciences and Engineering Research Council of Canada, Heart and Stroke Foundation of Canada, and Medical Research Council of Canada.

REFERENCES

Allard, L.; Langlois, Y.; Durand, L.-G.; Roederer, G. O.; Beaudoin, M.; Cloutier, G.; Roy, P.; Robillard, P. Computer analysis and

pattern recognition of Doppler blood flow spectra for disease classification in the lower limb arteries. Ultrasound Med. Biol. 17:211–223; 1991.

Allard, L.; Langlois, Y. E.; Durand, L.-G.; Roederer, G. O.; Cloutier, G. Effect of ensemble averaging on amplitude and feature variabilities of Doppler spectrograms recorded in the lower limb arteries. Med. Biol. Eng. Comput. 30:267–276; 1992.

Allard, L.; Cloutier, G.; Durand, L.-G.; Roederer, G. O.; Langlois, Y. E. Limitations of ultrasonic scanning for diagnosing lower limb arterial stenoses in the presence of adjacent segment disease. J. Vasc. Surg. 19 (in press); 1994.

Bascom, P. A. J.; Cobbold, R. S. C.; Routh, H. F.; Johnston, K. W. On the Doppler signal from a steady flow asymmetrical stenosis model: Effects of turbulence. Ultrasound Med. Biol. 19:197–210; 1993.

Cannon, S. R.; Richards, K. L.; Rollwitz, W. T. Digital Fourier techniques in the diagnosis and quantification of aortic stenosis with pulse-Doppler echocardiography. J. Clin. Ultrasound 10:101–107; 1982.

Choi, H.; Williams, W. J. Improved time-frequency distribution of multicomponent signals using exponential kernels. IEEE Trans. Acoust. Speech, Signal, Processing 37:862–871; 1989.

Cloutier, G.; Lemire, F.; Durand, L.-G.; Latour, Y.; Langlois, Y. E. Computer evaluation of Doppler spectral envelope area in patients having a valvular aortic stenosis. Ultrasound Med. Biol. 16:247–260; 1990.

Cloutier, G.; Lemire, F.; Durand, L.-G.; Latour, Y.; Jarry, M.; Soignac, A.; Langlois, Y. E. Change in amplitude distributions of Doppler spectrograms recorded below the aortic valve in patients with a valvular aortic stenosis. Ultrasound Med. Biol. 17:667–678; 1991.

Cohen, J. A coefficient of agreement for normal scales. Educ. Psych. Meas. 20:37–46; 1960.

Durand, L.-G.; Blanchard, M.; Sabbah, H. N.; Hamid, M. S.; Kemp, S. R.; Stein, P. D. A Bayes model for automatic detection and quantification of bioprosthetic valve degeneration. Math. Comput. Modelling 11:158–163; 1988.

Gonzalez, R. C.; Wintz, P. Chapter 7: Image segmentation and description. In: Digital image processing. Reading, MA: Addison-Wesley Publishing Company; 1977:354–358.

Guo, Z.; Durand, L.-G.; Allard, L.; Cloutier, G.; Lee, H. C.; Langlois, Y. E. Cardiac Doppler blood flow signal analysis, Part I: Evaluation of the normality and stationarity of the temporal signal. Med. Biol. Eng. Comput. 31:237–241; 1993a.

Guo, Z.; Durand, L.-G.; Allard, L.; Cloutier, G.; Lee, H. C.; Langlois, Y. E. Cardiac Doppler blood flow signal analysis, Part II: The time-frequency distribution by using autoregressive modeling. Med. Biol. Eng. Comput. 31:242–248; 1993b.

Guo, Z.; Durand, L. G.; Lee, H. C. The time-frequency distributions of nonstationary signals based on a Bessel kernel. IEEE Trans. Signal Processing (in press); 1994a.

Guo, Z.; Durand, L.-G.; Lee, H. C. Comparison of time-frequency distribution techniques on simulated Doppler ultrasound signal of the femoral artery. IEEE Trans. Biomed. Eng. (in press); 1994b.

Jager, K. A.; Phillips, D. J.; Martin, R. L.; Hanson, C.; Roederer, G. O.; Langlois, Y. E.; Ricketts, H. J.; Strandness, D. E., Jr. Noninvasive mapping of lower limb arterial lesions. Ultrasound Med. Biol. 11:515–521; 1985.

Jain, A. K. Advances in statistical pattern recognition. In: Pattern recognition theory and applications. F30. Berlin: Springer-Verlag; 1987:1–19.

Jeong, J.; Williams, W. Kernel design for reduced interference distributions. IEEE Trans. Signal Processing 40:402–412; 1992.

Kashyap, R. L.; Chellappa, R. Stochastic models for closed boundary analysis: Representation and reconstruction. IEEE Trans. Inform. Theory IT-27:627–637; 1981.

Kay, S. M.; Marple, S. L. Spectrum analysis—a modern perspective. Proceedings of the IEEE. 69:1380–1419; 1981.

Kohler, T. R.; Nance, D. R.; Cramer, M. M.; Vandenburghe, N.; Strandness, D. E. Duplex scanning for diagnosis of aortoiliac and femoropopliteal disease: A prospective study. Circulation 76:1074–1080; 1987.

Kohler, T. R.; Andros, G.; Porter, J. M.; Clowes, A.; Goldstone, J.; Johansen, K.; Raker, E.; Nance, D. R.; Strandness, D. E. Can Duplex scanning replace arteriography for lower extremity arterial disease? Ann. Vasc. Surg. 4:280–287; 1990.

Mo, L. Y. L.; Yun, L. C. M.; Cobbold, R. S. C. Comparison of four digital maximum frequency estimators for Doppler ultrasound. Ultrasound Med. Biol. 14:355–363; 1988.

Moneta, G. L.; Yeager, R. A.; Antonovic, R.; Hall, L. D.; Caster, J. D.; Cummings, C. A.; Porter, J. M. Accuracy of lower extremity arterial duplex mapping. J. Vasc. Surg. 15:275–284; 1992.

Oliviero, A.; Scarpetta, G. A new approach to contour coding. Comput. Graph. Image Processing 15:87–92; 1981.

Persoon, E.; Fu, K. S. Shape discrimination using Fourier descriptors. IEEE Trans. System, Man, Cybern. SMC-7:170–179; 1977.

Ranke, C.; Creutzig, A.; Alexander, K. Duplex scanning of the peripheral arteries: Correlation of the peak velocity ratio with angiographic diameter reduction. Ultrasound Med. Biol. 18:433–440; 1992.

Taylor, K. J. W.; Burns, P. N.; Wells, P. N. T. Clinical applications of Doppler ultrasound. New York: Raven Press; 1988:331–332.

Toussaint, G. T. Bibliography on estimation of misclassification. IEEE Trans. Inform. Theory IT-20:472–479; 1974.

Vaitkus, P. J.; Cobbold, R. S. C.; Johnston, K. W. A comparison study and assessment of Doppler ultrasound spectral estimation techniques, Part II: Methods and results. Ultrasound Med. Biol. 14:673–688; 1988.

Wallace, T. P.; Wintz, P. A. An efficient three-dimensional aircraft recognition algorithm using normalized Fourier descriptors. Comput. Graph. Image Processing 13:99–126; 1980.